Eur. Phys. J. E **26**, 405–409 (2008)
DOI 10.1140/epje/i2008-10336-1

THE EUROPEAN PHYSICAL JOURNAL E

Bridging dielectric fluids by light: A ray optics approach

R.D. Schroll[1], E. Brasselet[2,a], W.W. Zhang[1], and J.-P. Delville[2]

[1] Physics Department and the James Franck Institute, University of Chicago, 929 East 57th Street, Chicago, Illinois 60637, USA
[2] Centre de Physique Moléculaire Optique et Hertzienne, Université Bordeaux I, CNRS, 351 Cours de la Libération, 33405 Talence Cedex, France

Received 11 March 2008 and Received in final form 7 May 2008
Published online: 20 June 2008 –

Abstract. Rayleigh-Plateau instability is known to impose a stability limit for the length of a liquid bridge in weightless conditions. This fundamental limit may be exceeded by using a light field to form and stabilize dielectric fluid bridges (A. Casner, J.P. Delville, Europhys. Lett. **65**, 337 (2004)). Using both new experimental data as well as a new theoretical approach, we show that both the size and the stability of such light-sustained dielectric bridge can be qualitatively explained. We present a ray optics model that encompasses the competition between surface tension effects and optical radiation pressure arising from total internal reflection inside the bridge. A critical power below which a liquid bridge can no longer be sustained by light is predicted and confirmed experimentally. The observed power dependence of the bridge diameter also agrees with the proposed stabilization mechanism.

PACS. 47.20.Ma Interfacial instabilities (e.g., Rayleigh-Taylor) – 42.25.Gy Edge and boundary effects; reflection and refraction – 42.50.Wk Mechanical effects of light on material media, microstructures and particles – 82.70.Kj Emulsions and suspensions

Introduction

Liquid bridges are free-standing fluid cylinders of finite volume surrounded by a second fluid and stabilized between two solid surfaces by surface tension. They play an important role in many different areas of science going from crystal growth by the floating zone method [1], to micro total analysis system applications [2]. However, control and stabilization of large-aspect-ratio liquid bridges is very challenging [3]. Beyond a certain aspect ratio $\Lambda = \ell/2R$, where ℓ is the height and $2R$ the diameter, liquid columns are known to break into droplets due to the Rayleigh-Plateau instability [4]. This behavior, investigated for more than a century [5] is still under intense research because, up to now, advanced methods used to bypass the Rayleigh-Plateau limitation almost failed in stabilizing liquid columns with large aspect ratios. In weightless conditions, a cylindrical liquid column becomes unstable and breaks when its length exceeds its circumference (*i.e.* $\Lambda > \pi$); buoyancy even lowers this value of the aspect ratio onset. Gravity was then compensated by magnetic fields [6]. Further increase of the instability onset was investigated under axial and radial electric fields for both dielectric [7] and conducting [8] liquids. Passive [9] and active [10] control by acoustic radiation pressure was also demonstrated. Despite a large amount of efforts, the largest value reached was $\Lambda = 5$ [11]. In a recent work [12], we experimentally demonstrated that the optical radiation pressure was able to stabilize liquid bridges well above the Rayleigh-Plateau onset (a picture was given for $\Lambda = 14$). Aside from this fundamental fluid mechanics aspect, the method also seems promising in micro-technologies because laser-sustained liquid columns are tunable in aspect ratio, adjustable in direction and totally reconfigurable. Consequently, the range of applications is very wide, going from micro-optics (*i.e.* liquid columns behave as soft optical fibers) to microfluidic pipes, as fluid transfer can be optically controlled and directed in three dimensions [13]. This investigation nevertheless needed theoretical insights in order to understand why light beams are able to stabilize liquid columns so easily while classical electric and acoustic fields are unable to do so. This is the purpose of the present work.

We study the size and the stability of dielectric fluid bridges sustained by light and propose a simple geometrical model that grasps the main features of the observations. The main idea is to balance the competing radial effects of surface tension, which tends to break the

[a] e-mail: e.brasselet@cpmoh.u-bordeaux1.fr

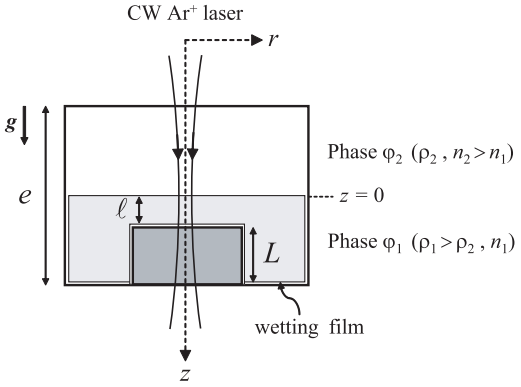

Fig. 1. Sketch of the experimental set-up. The TEM_{00} mode of a CW argon ion laser operating at 514.5 nm is focused at the fluid-fluid interface of the phase-separated liquid mixture whose temperature is regulated above the critical temperature T_c. The less refractive phase φ_1 (density ρ_1, refractive index n_1) is the denser one. The cell thickness is $e = 2\,\text{mm}$ and the working thickness is $\ell = 200\,\mu\text{m}$, which is calibrated by introducing a glass slab of thickness $L = 800\,\mu\text{m}$ at the bottom of the cell.

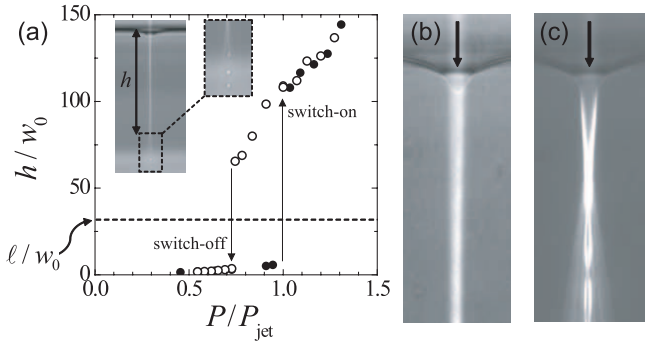

Fig. 2. (a) The maximum height h of the light-induced deformation for increasing (filled circles) and decreasing (open circles) power. The laser power P is normalized by the value P_{jet}. Above P_{jet} the downward deformation transforms discontinuously into a fluid jet (inset). The dashed line indicates the lower-layer depth ℓ used in the bridge experiment (see Fig. 1). (b,c) Formation of fluid jet. At $t = 0$, the laser power is increased to $P = 460\,\text{mW}$, a value above P_{jet}. The beam waist is $w_0 = 3.5\,\mu\text{m}$ and $T - T_c = 5\,\text{K}$. (b) At $t = 1.2\,\text{s}$, the interface forms a downward deflection. (c) At $t = 7.2\,\text{s}$, the interface has evolved into a liquid jet and the scattering of the resulting light guiding by the jet edges is visible.

bridge through Rayleigh-Plateau instability, and optical radiation pressure arising from total internal reflection inside the bridge that helps to keep the bridge open. We predict the existence of a threshold power below which a liquid bridge can no longer be sustained by light, as is seen in the experiments. The power dependence of the bridge diameter also agrees with the proposed stabilization mechanism.

Experiments and results

The experimental set-up is depicted in Figure 1. It consists of a phase-separated near-critical liquid mixture contained in a thermo-regulated glass cell at temperature T, for which a very low surface tension can be obtained. Details on the preparation of the solution can be found in [14]. Above the critical temperature $T_c \simeq 35\,^\circ\text{C}$, two distinct phases φ_1 and φ_2 of different composition coexist. The densities and refractive indices satisfy $\rho_1 > \rho_2$ and $n_1 < n_2$, respectively. Therefore the phase φ_1, of lowest refractive index, is at the bottom of the cell. In addition, the phase φ_2 completely wets the cell walls close to T_c, forming a wetting layer at the bottom of the cell. A vertical downward TEM_{00} Gaussian beam from a CW Ar^+ laser operating at wavelength $\lambda = 514.5\,\text{nm}$ is focused at normal incidence onto the fluid-fluid interface, along the z-axis, as shown in Figure 1. The intensity profile at the unperturbed interface is

$$I(r) = \frac{2P}{\pi w_0^2} \exp\left(-2r^2/w_0^2\right), \qquad (1)$$

where r is the radial distance from the centerline of the laser beam, P is the total beam power and w_0 is the beam waist. Since $n_1 < n_2$, the raditation pressure exerted by the laser beam deforms the interface downward [15] (Fig. 2(a)). When the laser power exceeds a critical value P_{jet}, the interface deforms into a fluid jet, with droplets emitted from the end of the jet (see inset of Fig. 2(a)) [16].

The jet structure results from an opto-hydrodynamic instability whose proposed mechanism is the destabilization of the small-amplitude surface deformation as the beam experiences total internal reflection at the inflexion point location, where the local incidence angle of light θ_{inc} at the interface is the largest [16]. Indeed, as $n_2 > n_1$, light incident from phase φ_2 is totally reflected and directed toward the deformation tip if $\theta_{\text{inc}} > \theta_c = \arcsin(n_1/n_2)$. The dynamical scenario of the jetting instability is illustrated in Figures 2(b, c) with snapshots at time $t = 1.2\,\text{s}$ (a) and $t = 7.2\,\text{s}$ (b) when laser is switched on at $t = 0$ with $P > P_{\text{jet}}$. When power is decreased, a hysteresis loop is observed and the large deformation is sustained at power $P < P_{\text{jet}}$ until it suddenly switches back to the small-amplitude deformation regime. Then, if the initial thickness of the phase φ_1 is smaller than the jet length h, a bridge forms between the interface and the wetting layer.

For our purpose, we want to obtain bridges instead of jets for all laser power values $P > P_c$. This is ensured by choosing the working thickness ℓ to lie below the switch-off height, which corresponds to $h/w_0 \sim 60$ (Fig. 2(a)). In practice we chose $\ell = 200\,\mu\text{m}$, which is calibrated introducing a glass slab of thickness $L = 800\,\mu\text{m}$ at the bottom of the cell of thickness $e = 2\,\text{mm}$ containing the phase φ_1 to a height of 1 mm (Fig. 1). This corresponds to $\ell/w_0 \sim 30$ for the experimental data presented here, where $w_0 = 6.95\,\mu\text{m}$ (except for Fig. 2 where $w_0 = 3.5\,\mu\text{m}$), and therefore we shall refer to P_{bridge} instead of P_{jet} for clarity in what follows. Experiments were carried out at fixed temperature $T - T_c = 4\,\text{K}$ (except for Fig. 2 where $T - T_c = 5\,\text{K}$) for which we have

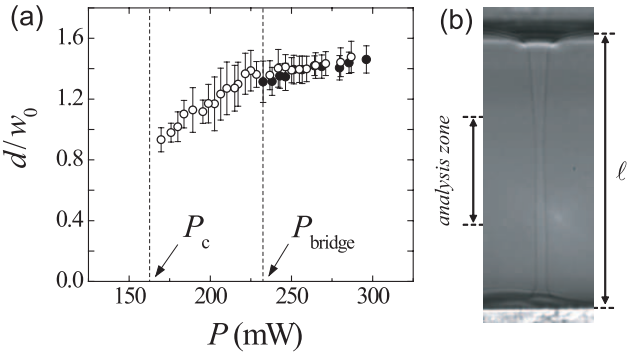

Fig. 3. (a) Bridge diameter as a function of power for $w_0 = 6.95\,\mu$m for increasing (filled circles) and decreasing (open circles) power. P_c is the critical power below which the bridge is no longer stabilized by light. (b) Typical bridge obtained at 230 mW. The aspect ratio is $\Lambda \approx 20$.

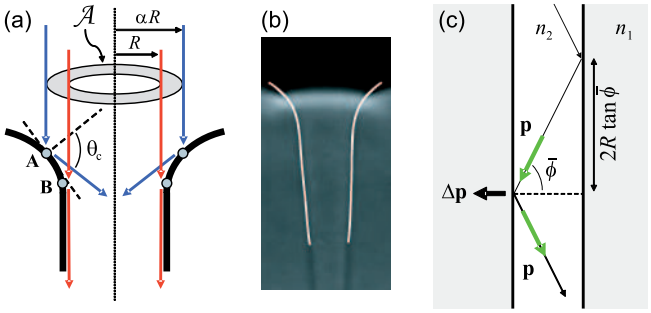

Fig. 4. (Color online). Illustration of the geometrical model of optical bridge stabilization. (a) Rays impinging on the interface at an angle larger than θ_c, the critical angle for total internal reflection, participate in stabilizing the bridge structure. (b) Picture of the funnel shape at the bridge entrance showing data analysis (white line) from which the parameter α is estimated. (c) Linear momentum transfer $\Delta\mathbf{p}$ of a photon that undergoes total internal reflection inside the bridge.

$n_1 = 1.442$, $n_2 = 1.462$ and a surface tension value $\sigma = 4.20 \times 10^{-7}\,\mathrm{J/m^2}$ [17]. The power dependence of the bridge diameter d is obtained by analyzing the central part of the bridge picture. It is illustrated in Figure 3 where filled (open) symbols correspond to increasing (decreasing) power. Let us note finally that laser beams are indeed able to stabilize bridges which would be unstable otherwise. This can easily be demonstrated by removing the optical excitation; Rayleigh-Plateau rupture occurs systematically.

Geometrical model

We next show that the main features associated with the onset of the bridge structure are captured by a simple model, in which the constricting effect of surface tension is balanced by the radiation pressure generated by light reflecting off the bridge surface. Since the bridge radius is larger than the wavelength of the light, we adopt here the simplest approach and model the propagation and the reflection of the light within the bridge via geometric optics. While this is strictly correct only when the bridge radius is much larger than the wavelength of light, it is sufficient to reproduce the main observed features.

We model the bridge as a cylinder of radius R aligned with the beam. As the Rayleigh range of the incident beam, $\pi w_0^2/\lambda$, is of the order of or larger than the bridge length, we can consider the laser light to be shining directly downwards, without any radial spreading. Thus, from a geometrical optics view, the light shining directly into the bridge will not interact with the walls. Light at a radius larger than R is reflected off the interface and directed into the bridge. Since the index of refraction inside the bridge is larger than the index of the surrounding fluid, some of this light may be trapped inside the bridge by total internal reflection. We assume that the total power trapped in this manner, denoted $P_{\mathcal{A}}$, is equal to the power shining on the interface at a radius between R and αR ($\alpha > 1$). This is illustrated in Figure 4(a), where light falling between points A and B is reflected into the bridge. Thus,

$$P_{\mathcal{A}} = 2\pi \int_R^{\alpha R} I(r) r \mathrm{d}r, \\ = P e^{-\frac{2R^2}{w_0^2}} \left(1 - e^{-\frac{2(\alpha^2-1)R^2}{w_0^2}}\right). \quad (2)$$

The parameter α is defined such that rays impinging on the funnel at radius αR have an impact angle of θ_c, the critical angle for total internal reflection. This parameter is estimated by analyzing the actual shape of the bridge funnel. We measure $\alpha_{\mathrm{exp}} = 2.13$ for $w_0 = 6.95\,\mu$m (see Fig. 4(b)), which is almost constant within the investigated range of waists.

Once the reflected light enters the bridge, it will bounce down the bridge at some angle $\phi > \theta_c$ to the normal. Since the optical indices of the two fluids are similar, θ_c is close to $\pi/2$. More precisely, at $T - T_c = 4\,\mathrm{K}$, we have $\theta_c \simeq 81.4°$. Thus, a reasonable approximation is that all of the light reflects at the same angle $\bar{\phi}$ and, further, that this angle can be approximated as

$$\bar{\phi} = \frac{1}{2}\left(\theta_c + \frac{\pi}{2}\right). \quad (3)$$

As each trapped photon of energy E_γ reflects off of the bridge interface, its linear momentum changes by

$$\Delta p = \|\mathbf{p}^+ - \mathbf{p}^-\| = 2\frac{n_2}{c} E_\gamma \cos\bar{\phi}\,. \quad (4)$$

The bridge interface receives an equal impulse in the outwards normal direction (see Fig. 4(c)). The total radiation pressure on the bridge surface is given by the product of the momentum change per photon, Δp, by the number of reflections per unit area of the bridge wall. For photons reflecting at an angle $\bar{\phi}$, this reflection density is given by the rate of photons $P_{\mathcal{A}}/E_\gamma$ divided by the area per reflection for a single photon, $4\pi R^2 \tan\bar{\phi}$. Thus, the radiation

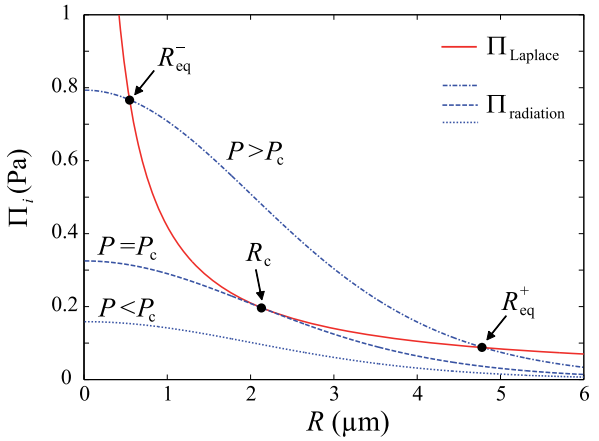

Fig. 5. (Color online). Laplace pressure (solid line) and radiation pressure for $P < P_{\rm c}$ (dotted line), $P = P_{\rm c}$ (dashed line) and $P > P_{\rm c}$ (dash-dotted line), as a function of the bridge radius R.

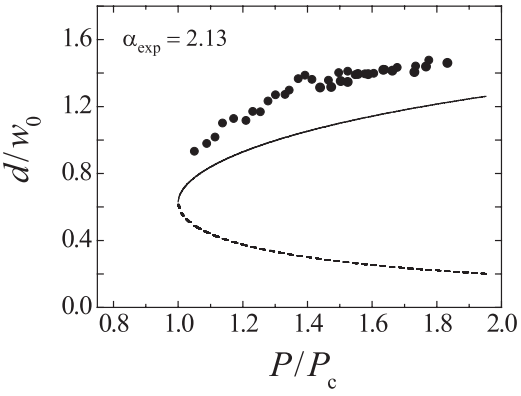

Fig. 6. Comparison between the model and experimental results for $w_0 = 6.95\,\mu$m and $T - T_{\rm c} = 4\,$K. Solid (dashed) line corresponds to stable (unstable) states and circles are the experimental results.

pressure is given by

$$\Pi_{\rm radiation} = \frac{P_{\mathcal{A}}/E_\gamma}{4\pi R^2 \tan\overline{\phi}}\Delta p = \frac{n_2}{2c}\frac{\cos\overline{\phi}}{\tan\overline{\phi}}\frac{P_{\mathcal{A}}}{\pi R^2}\,. \qquad (5)$$

Given equation (3) and $n_1 \approx n_2$, we can expand in the difference between the indices to find $\cos\overline{\phi}/\tan\overline{\phi} \approx (n_2 - n_1)/2n_2$.

Then, from equation (5), we can calculate the bridge radius as a function of the laser power by balancing the radiation pressure $\Pi_{\rm radiation}$, which tends to expand a cylindrical bridge outwards, against the inward constricting stresses exerted by surface tension. Finally the equilibrium equation writes

$$\frac{\sigma}{R} = \frac{n_2 - n_1}{4c\pi}\frac{P_{\mathcal{A}}}{R^2}\,. \qquad (6)$$

In Figure 5 we plot the Laplace pressure $\Pi_{\rm Laplace} = \sigma/R$ due to surface tension and the radiation pressure $\Pi_{\rm radiation}$ as a function of the bridge radius R. As one can deduce graphically from Figure 5, the model predicts that there is i) no equilibrium radius for the bridge below a critical power $P_{\rm c}$, ii) a unique solution $R = R_{\rm c}$ at $P = P_{\rm c}$, and iii) a pair of equilibrium radii $(R_{\rm eq}^-, R_{\rm eq}^+)$, with $R_{\rm eq}^- < R_{\rm eq}^+$, when $P > P_{\rm c}$. In the latter case, surface tension is larger than radiation pressure for small R, since the area gathering light is so small, and also for large R, since the light is only being gathered from the dim tails of the intensity profiles. For $R_{\rm eq}^- < R < R_{\rm eq}^+$, enough light is captured that radiation pressure dominates. For the static balance to be stable against variation in the bridge radius, we must have $(\partial_R \Pi_{\rm radiation})(R_{\rm eq}) < (\partial_R \Pi_{\rm Laplace})(R_{\rm eq})$. This is only satisfied at $R = R_{\rm eq}^+$. Therefore, any bridge $R_{\rm eq}^- < R < R_{\rm eq}^+$ in this regime would be widened up to $R_{\rm eq}^+$, the stable equilibrium, and $R_{\rm eq}^-$ represents an unstable solution.

Discussion

We plot the model's predictions of bridge diameter as a function of the laser power and compare them against the measured bridge diameters in Figure 6. To faciliate the comparison, we have rescaled the bridge diameter by the size of the beam waist w_0 and the laser power by $P_{\rm c}$, the power below which no bridge exists. The simple model successfully captures all the qualitative features of bridge formation. In particular, it demonstrates the onset of a stable bridge when the laser power is sufficiently large, as well as a gradual widening of the bridge radius with power above $P_{\rm c}$. However, there is a discrepancy in the size of the bridge. The measured bridge is slightly wider than that predicted by our model. In addition, with the measured value $\alpha_{\rm exp}$, we can use the model to estimate the value of the critical power $P_{\rm c}$. By definition, the latter is determined from $\Pi_{\rm radiation}(R_{\rm c}) = \Pi_{\rm Laplace}(R_{\rm c})$ and $(\partial_R \Pi_{\rm radiation})(R_{\rm c}) = (\partial_R \Pi_{\rm Laplace})(R_{\rm c})$, where $R_{\rm c}$ is the equilibrium radius at $P = P_{\rm c}$. Then, the dependence of $P_{\rm c}$ on the beam waist w_0 is numerically calculated and compared to the measurements in Figure 7. The critical power scales linearly with the beam waist, consistently with the model, but there is again a quantitative offset. The model estimate is about a factor 2.5 larger than the experimental value. These quantitative discrepancies suggest that the crude assumptions employed in our simple model, *i.e.* that light propagation can be modelled by geometric optics and that all the light rays are reflected off the bridge surface with the same angle, are unable to capture the quantitative evolution of the bridge structure, although it suceeds in capturing the main qualitative features of the bridge formation.

Before concluding, we comment the influence of possible viscous stress on the bridge stability. In a previous work, we have shown that when ΔT is small, so that the experimental system is near the second-order phase transition, light scattering off the density fluctuations in the liquid imparts momentum to the liquid in the lit region, driving a flow inside the jet [13]. In the bridge regime, the scattering-driven flow is still present and exerts a viscous

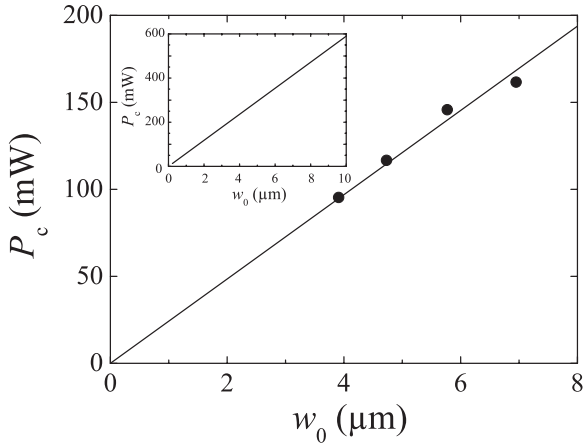

Fig. 7. The scaling of the critical power P_c with the beam width w_0 at $T - T_c = 4\,\mathrm{K}$. Inset shows the predicted scaling from the geometric optics model. The linear trend is correctly predicted, although the overall scale is off.

stress on the interface. We can estimate the viscous stress as follows. From our prior work, we know that a laser beam of power P gives rise to a downward flow within the jet with typical velocity u_z. Estimates of u_z from the experiments give values in the range 10–100 μm/s. Because a liquid bridge is not perfectly cylindrical along its entire length in practice, the downward light-driven flow is accompanied by a secondary flow whose radial component u_r satisfies $u_r \sim u_z R/\ell$. This radial flow gives rise to a typical viscous stress $\mu u_r/R = \mu u_z/\ell$ onto the bridge surface, where μ is the mean shear viscosity (close to T_c one has $\mu_1 \simeq \mu_2$). We can gauge the relative importance of the viscous stress to the dominant stress balance keeping the bridge open (Eq. (6)) from the dimensionless ratio between the viscous stress and the surface tension pressure. This corresponds to a capillary number

$$Ca = \frac{\mu u_z R}{\sigma \ell}\,. \tag{7}$$

The bridge experiments analyzed here span *Ca* values from 10^{-3} to 10^{-2}, thus confirming the basic assumption in our simple model that the bridge observed is governed by a static force balance.

Conclusion

The main motivation of the present work was to give some theoretical insights on the mechanism by which radiation pressure allows for liquid bridges stabilization well above the Rayleigh-Plateau onset, contrary to other external forcing. Since the optical specificity of liquid bridges is to behave intrinsically as waveguides, we suspected this guiding to be at the origin of the observed stabilization. To check this hypothesis, we used a ray optics description of the light trapped in the bridge and investigate the competition between the radiation pressure of the guided photons and the Laplace pressure. This model has then been compared to new experiments. All predictions of our model are retrieved experimentally, *i.e.* i) existence of equilibrium between competing radial contributions of optical radiation pressure and surface tension, and ii) emergence of a beam power onset below which no stabilization is possible. The quantitative comparison shows a mismatch in the value of this onset, but we have to remember that our ray optics approach and its subsequent ray selection mechanism by the funnel of the bridge are only a partial picture of a more complicated electromagnetism problem. However, since a simple ray optics description predicts the right behaviors, it can be considered as the first step toward a proper analytical description of laser-sustained large-aspect-ratio liquid bridges.

We are grateful to R. Wunenburger for fruitful comments and to C. Loumena for experimental support. This work was partly supported by the CNRS and the Conseil Régional d'Aquitaine, and by the National Science Foundation (R.D.S.), NSF Contract No. CBET-0730629 (W.W.Z.).

References

1. J. Meseguer, J.M. Perales, I. Martinez, N.A. Bezdenejnykh, A. Sanz, Curr. Topics Crystal Growth Res. **5**, 27 (1999).
2. M. Wu, T. Cubaud, C.-M. Ho, Phys. Fluids **16**, L51 (2004).
3. W. Wei, D.B. Thiessen, P.L. Marston, Phys. Rev. E **72**, 067304 (2005).
4. J. Eggers, Rev. Mod. Phys. **69**, 865 (1997).
5. J. Plateau, Ann. Phys. Chem. **80**, 566 (1850).
6. M.P. Mahajan, S. Zhang, M. Tsige, P.L. Taylor, C. Rosenblatt, J. Colloid Interface Sci. **213**, 592 (1999).
7. C.L. Burcham, D.A. Saville, J. Fluid Mech. **405**, 37 (2000).
8. M.J. Marr-Lyon, D.B. Thiessen, F.L. Blonigen, P.L. Marston, Phys. Fluids **12**, 986 (2000).
9. M.J. Marr-Lyon, D.B. Thiessen, P.L. Marston, Phys. Rev. Lett. **86**, 2293 (2001); **86**, 2293 (2001)(E).
10. M.J. Marr-Lyon, D.B. Thiessen, P.L. Marston, J. Fluid Mech. **351**, 345 (1997).
11. H. Gonzales, F.M.J. McCluskey, A. Castellanos, A. Barrero, J. Fluid. Mech. **206**, 545 (1989).
12. A. Casner, J.P. Delville, Europhys. Lett. **65**, 337 (2004).
13. R.D. Schroll, R. Wunenburger, A. Casner, W.W. Zhang, J.P. Delville, Phys. Rev. Lett. **98**, 133601 (2007).
14. A. Casner, J.P. Delville, Phys. Rev. Lett. **87**, 054503 (2001).
15. R. Wunenburger, A. Casner, J.P. Delville, Phys. Rev. E **73**, 036314 (2006).
16. A. Casner, J.P. Delville, Phys. Rev. Lett. **90**, 144503 (2003).
17. H. Chraïbi, D. Lasseux, E. Arquis, R. Wunenburger, J.-P. Delville, Eur. J. Mech. B/Fluids **27**, 419 (2008).